Nanotribology of transition metal dichalcogenide flakes deposited by chemical vapour deposition: the influence of chemical composition and sliding speed on nanoscale friction of monolayers

Ales Rapuc*[1], He Wang[1], and Tomas Polcar†[1,2]

[1]National Centre for Advanced Tribology, Faculty of Engineering and Physical Sciences, University of Southampton, Southampton SO17 1BJ, United Kingdom
[2]Department of Control Engineering, Faculty of Electrical Engineering, Czech Technical University in Prague, Technicka 2, 16627 Prague 6, Czech Republic

Abstract

We present nanoscale frictional analysis of three commonly used transition metal dichalcogenide (TMD) monolayers, WS_2, $MoSe_2$ and WSe_2, deposited by chemical vapour deposition (CVD). The monolayers were characterised by Raman spectroscopy, photoluminescence spectroscopy (PL), and X-Ray spectroscopy (XPS), to determine the composition of the coating and confirm monolayer structure. Nanoscale frictional analysis was performed by atomic force microscopy (AFM). Load-dependent frictional behaviour was measured at different sliding speeds to quantitatively assess friction on each sample. All samples experienced low nanoscale friction, with the lowest friction observed on WSe_2. The friction was independent of sliding speed within the analysed range. Furthermore, monolayer TMDs significantly increase the operational load range by at least one order of magnitude when compared to SiO_2 substrate.

Keywords: Transition metal dichalcogenides, Atomic force microscopy, Nanotribology, Monolayers, Chemical vapour deposition

1 Introduction

The experimental discovery of graphene in 2004 [1] and increased fabrication capabilities in the subsequent years [2, 3] have led to an increase in the applications and research interest related to atomically thin 2D nanomaterials, including transition metal dichalcogenides (TMDs) and hexagonal boron nitride, as well as more complex structures such as carbon nanotubes [4]. Besides their more conventional applications in nano-electronics, photonics and sensing [5–7], 2D nanomaterials have also emerged as a promising candidate for modifying friction on the nanoscale [8]. In particular, the undesirable properties of Si-Si contacts present an operational challenge in the performance of micro/nano-electro mechanical systems (MEMS/NEMS) [9–12]. Coating the contacting surfaces of these systems with 2D materials can provide a solution due to their favourable adhesion and frictional properties [13]. Understanding the behaviour of such materials within the small-scale contacts, namely the effects of friction and adhesion on their performance and wear, will help with further development of related materials and with the design of new components and systems incorporating them.

*a.rapuc@soton.ac.uk
†t.polcar@soton.ac.uk

Table 1: Nano-frictional properties of different materials.

Material	Atmosphere	$\tilde{\mu}$ [1] ($GPa^{1/3}$)	τ [2] (MPa)	Ref.
Amorphous carbon	Air	0.450±0.042	/	[30]
Amorphous carbon	Argon	0.158±0.022	/	[30]
Diamond	Air	0.158±0.061	/	[30]
Diamond	Argon	0.263±0.060	/	[30]
C60	Argon	0.67±0.22	/	[30]
HOPG	Argon	0.0012±0.0009	/	[30]
GeS	Air	0.50±0.21	/	[31]
Mica	Air	0.14±0.05	/	[31]
Mica	Argon	0.16±0.04	/	[31]
W-S-C coating	Air	/	36-91.2	[28]
W-S-C:Cr coating	Air	/	71-99.3	[27]

[1] Effective coefficient of friction for point-like contact
[2] Contact shear strength

Group 6 transition metal dichalcogenides (e.g., MoS_2, WS_2, $MoSe_2$, WSe_2 ...) are not new materials in the field of tribology. The patents involving the use of MoS_2 in technical applications date as far back as the late-1920s [14]. MoS_2 and WS_2 have been widely applied and studied as thin coatings for space applications since 1960s [15, 16] and extensively investigated throughout 1970s and 1980s [17, 18]. However, it was not until recently [19] that they have started receiving increasing interest as a material for reducing friction on the nanoscale. The low friction of bulk and multi-layered TMD systems is attributed to their lamellar structure, where weak van der Waals forces between the layers provide low shear resistance [20, 21]. On the other hand, low friction between a single monolayer and a second body is a result of surface inertness [22].

Atomic force microscopy (AFM) is a powerful tool for probing surface properties, such as adhesion and friction. Due to a small tip size, it can be used to mimic a single nanoscale asperity contact [23], therefore offering a wide array of nanotribological investigations. AFM has been previously successfully employed to study nano- and atomic- scale tribological properties of several different 2D systems: graphite [24], graphene [19, 25], exfoliated TMDs [19, 26], sputtered TMDs [27, 28] or h-BN [19]. However, most of the above studies only focused on a specific normal force and solely observed the trends within the same sample, such as the influence of the number of layers on friction [19, 26], sample orientation [24], or the effect of substrate morphology [29].

In the framework of this work, we are interested in using AFM to study how the elemental structure of the TMD monolayer influences nanoscale friction between the bare silicon tip and the TMD surface. Due to different tools, methods, equipment, and sample preparation being used in various studies, a direct quantitative comparison between the frictional response of TMD materials from literature is almost impossible. To quantitatively compare the data of different TMD samples, we deposited WS_2, $MoSe_2$ and WSe_2 monolayer flakes by an almost identical CVD procedure, and performed the analysis using the same setup (e.g., using the same probe, performing the measurements in a single session), thus minimising the external effects on the measurement. We present quantitative values of load-dependent friction behaviour on three major TMD monolayers ($MoSe_2$, WS_2 and WSe_2), according to Hertz-plus-offset model [30], which has been previously successfully applied to study nanoscale frictional properties and contact shear strength of many different materials (see Table 1). We used bare silicon tips, which offer a good depiction of a nanoscale tribo-system and accurately represent a contact in MEMS [12]. Furthermore, we examine the influence of sliding speed on nanoscale friction and compare how wear resistance and maximum applicable load differ between the TMD sample and the bare SiO_2 substrate.

Table 2: CVD deposition parameters.

Material	Precursors		Temperature for precursors T_1(°C)	T_2(°C)	Gas inlet	Note
$MoSe_2$	MoO_3	Se	750	300	H_2/Ar	
WS_2	WO_3	S	900	200	Ar	NaCl used
WSe_2	WO_3	Se	900	300	H_2/Ar	

2 Materials and methods

2.1 Synthesis of TMDs

The transition metal dichalcogenide monolayer samples (WS_2, $MoSe_2$, WSe_2) were deposited by chemical vapour deposition (CVD) on 300 nm SiO_2/Si substrate. The reaction was carried out in a 3 cm diameter quartz tube under atmospheric pressure. The substrates were loaded on a boat containing MoO_3 (or WO_3) (Alfa Aescar, 99.9995% purity) and placed in the tube centre. NaCl was added during the deposition of WS_2, to lower the high melting point of WO_3 and aid the vaporisation. Afterwards, another boat with sulphur (or selenium) (Alfa Aescar, 99.9995% purity) was placed at the upstream. After a 10 minute purge with 300 sccm Ar (or H_2/Ar) (BOC, 99.999% purity), the flow rate was reduced to 30 sccm, and the furnace was programmed to heat the substrates (T_1 in Table 2). Concurrently, sulphur (or selenium) was heated (T_2 in Table 2), allowing its vapour to be transported to the substrate. The furnace was switched off after 15 minutes of deposition and naturally cooled-down.

2.2 Characterisation of synthesised TMDs

Atomic force microscopy (AFM, Agilent Technologies, USA) was used to measure the surface morphology and flake thickness. The thickness of the flakes was measured in non-contact AFM mode. Raman spectroscopy (InVia Raman Spectrometer, 532 nm laser) was utilised to characterise the vibrational modes as well as photoluminescence (PL) spectra, and X-ray photoelectron spectroscopy (XPS, Thermo Scientific Theta Probe XPS System MC03, Al Kα source) was used to analyse the elemental composition of the flakes.

2.3 Friction and nanoscale wear measurement by AFM

Surface friction maps and topography were collected simultaneously by AFM (Agilent 5500, Agilent Technologies, USA) in contact mode. Frictional maps were used to examine the qualitative frictional contrast between the TMD sample and the substrate. We used a PPP-LFMR (Nanosensors, USA) probe at low contact loads and 1 Hz scan rate.

Load dependent frictional behaviour was measured using the same setup. A single PPP-LFMR probe was used to perform all the measurements, with the purpose of reducing measurement error due to discrepancies in the probe shape, calibration factors, or probe mounting. The normal spring constant was determined in-situ using a built-in thermal noise method [32] ($k = 0.109$ N/m). Lateral forces were calibrated according to the wedge calibration method [33] on commercial TGF11 (µMasch, Bulgaria) gratings ($\alpha = 278$ nN/V).

Measurements with incremental increasing or decreasing normal load were performed at three different sliding speeds (0.5, 1.0 and 1.5 µm/s) over 0.5 x 0.5 µm area. A total of 10 different loads were used, including negative loads to study the behaviour between the tip and the sample at very low loads (see Table 3). The value of minimum load was determined empirically on each sample, as the lowest load at which the tip did not lose contact with the surface during continuous sliding. The value of applied negative load had to be lower than the force of adhesion to ensure that the tip does not snap out of contact due to local

Table 3: LFM experimental parameters.

Sample	F_{min} (nN)	F_{max} (nN)	$F_{pull-off}$ (nN)
WS_2	-0.6Fpull-off	30	7.5
$MoSe_2$	-0.7Fpull-off	30	11.4
WSe_2	-0.7Fpull-off	30	7.5

differences in adhesion, contact area, or surface roughness. A custom script was employed to automatically control contact loads and sliding speeds during the experiments.

Nanoscale wear was evaluated in terms of surface damage and wear caused to the tip. We used stiffer probes (PPP-NCH, $k = 51$ N/m), which allowed us to reach much higher contact pressure required to induce any changes on the surface. The loads up to 10 µN were used. As a reference, the measurements on the TMD flakes were compared to sliding on SiO_2.

3 Results

3.1 Sample characterisation

WS_2: The samples were characterised by Raman spectroscopy using a 532 nm laser. As displayed in Figure 1a, the 2LA (353.1 cm^{-1}) and A_{1g} (420.1 cm^{-1}) peaks are indicative for a monolayer [34, 35]. In addition, PL spectrum in Figure 1b shows an emission peak at 620.2 nm, further confirming monolayer WS_2 structure.

The XPS spectra of monolayer WS_2 flakes in Figure 1c and d display the W 4f peaks at 34.7 and 32.5 eV, which are assigned to the $4f_{5/2}$ and $4f_{7/2}$ orbitals of WS_2, respectively [36, 37]. The W 5p core level at 37.4 eV suggests the existence of W^{6+}, likely residual WO_3 on the as-deposited sample [38]. 163.5 and 162.3 eV peaks belong to the S doublets: $2p_{1/2}$ and $2p_{3/2}$ [36]. All the results are indicative of WS_2 crystal with the atomic ratio between W and S of ∼1:2.

$MoSe_2$: The lateral sizes of the CVD deposited $MoSe_2$ nanoflakes were approximately 10-30 µm. Raman peaks at 238.3 cm^{-1} and 285.2 cm^{-1} (Figure 2a) were related to A_{1g} and E_{2g} modes, respectively [39, 40]. Additionally, we observed an unknown peak at 250.4 cm^{-1}. This peak can be often seen in the literature (see [40], [41] and [42]), but the authors did not comment on it. The 794.1 nm peak in the PL spectrum (Figure 2b) belongs to single-layer $MoSe_2$ [43, 44].

As evident from the XPS spectra in Figure 2c and d, the 232 and 228.8 eV peaks correspond to the Mo $3d_{3/2}$ and $3d_{5/2}$ orbitals, respectively; the Se 3d peaks at 54.9 and 54 eV originate from the $3d_{3/2}$ and $3d_{5/2}$ doublets [45, 46] . An atomic ratio of 1:2.05 is extracted for Mo and Se under this circumstance. Note that Raman spectroscopy was performed on the same sample as used later in AFM analysis, while PL and XPS spectra were obtained on a separate monolayer $MoSe_2$.

WSe_2: The lateral size of chemical vapour deposited triangular WSe_2 nanofilms was 5-20 µm. Two Raman peaks at 249.2 and 258.9 cm^{-1} belong to the E_{2g} and A_{1g} modes of WSe_2, respectively. As the van der Waals force can induce the interactions between neighbouring layers, a peak at ∼308 cm^{-1} can be detected for multi-layered WSe_2. Thus, the absence of this specific peak has been used to confirm the single-layer nature of WSe_2 instead of the frequency difference between E_{2g} and A_{1g} modes [47, 48]. Evidently, there is no B^1_{2g} peak at ∼308 cm^{-1} as demonstrated by the inset of Figure 3a, so we can conclude that the as-grown WSe_2 consists of a single layer. Additionally, the emission peak at 752.5 nm also indicates the single-layer nature of the WSe_2 sample (3b) [48].

As for the XPS spectra in Figure 3c and d, the peaks at 32.5 and 34.7 eV are the W $4f_{7/2}$ and W $4f_{5/2}$ doublets; the weak peak at 37.4 eV may result from the WO_3 residues on the sample surface; the 54.8 and 55.7 eV peaks are ascribed to the Se $3d_{5/2}$ and Se $3d_{3/2}$ orbits; the atomic ratio of W and Se was calculated to be 1:1.98, which is close to the stoichiometric 1:2 [49].

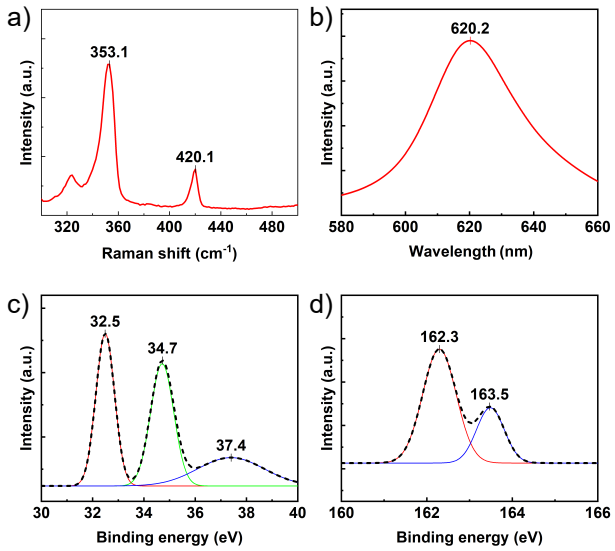

Figure 1: Characterisation of WS_2 nanoflakes synthesised on SiO_2/Si substrate by the CVD method. (a) Raman spectrum and (b) PL spectrum with 532 nm laser excitation. XPS spectra of (c) W 4f and (d) S 2p orbitals of a monolayer.

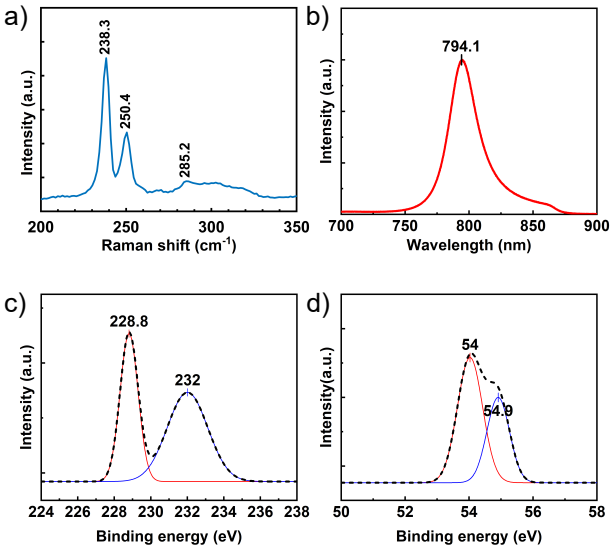

Figure 2: Characterisation of chemical vapour deposited $MoSe_2$ nanoflakes on SiO_2/Si substrate. (a) Raman spectrum and (b) PL spectrum with 633 nm laser excitation. XPS spectra of (c) Mo 3d and (d) Se 3d orbitals.

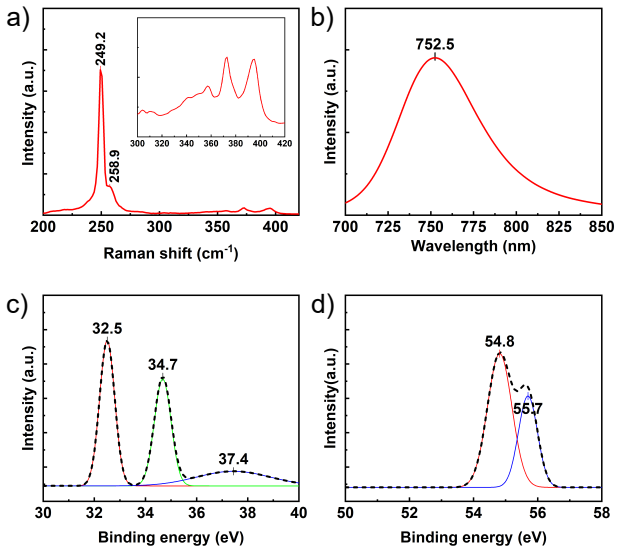

Figure 3: Characterisation of WSe_2 nanoflakes synthesised on SiO_2/Si substrate by CVD method. (a) Raman spectrum and (b) PL spectrum with 532 nm laser excitation. XPS spectra of (c) W 4f and (d) Se 3d orbitals of a monolayer.

3.2 Nanotribology: Friction maps and load-dependent frictional behaviour

The topography of the chosen WS_2, $MoSe_2$ and WSe_2 flakes for nanotribological analysis, together with their corresponding friction maps and load-dependent frictional response is shown in Figure 4. Note that the flakes presented in this section are not the exact same monolayers used for characterisation in the previous section, due to their small size and different methods used to characterise the samples. However, the flakes used for frictional experiments and for structural characterisation were taken from the same sample (i.e., from the same CVD batch), unless otherwise noted.

The surface topography of the specific flakes was obtained just before performing each friction experiment. As shown in Figure 4a, WS_2 and WSe_2 formed triangular crystals, indicating well-controlled crystal growth, while $MoSe_2$ resulted in 'snowflake-like' flake shape. Nevertheless, the scan on $MoSe_2$ displays triangular grain boundaries within the flake, thus indicating that the single grains are, in fact, triangular. The 'snowflake-like' shape is a consequence of recrystallisation due to longer deposition time [42]. We have checked the analysed flakes using Raman spectroscopy (see Figure 2a), which confirmed the monolayer structure. Furthermore, friction measurements on $MoSe_2$ were comparable with the other two (in absolute value and load-dependent behaviour), further ensuring the quality and crystallinity of the surface. For example, poor crystallinity or low crystal quality should result in increased friction due to the presence of dangling bonds.

The measured values of thickness vary substantially between the samples. WS_2 and $MoSe_2$ flakes show no height difference compared to the substrate, while the measured thickness of WSe_2 was 1.10 ± 0.12 nm. The same structure was observed on additional WS_2, WSe_2 and $MoSe_2$ flakes (Supporting Information, Figure S1), showing that the structure is comparable between the flakes on the same sample. We must note that because these measurements were performed in contact mode, the measured thickness can differ from the actual value. The discrepancy can be attributed to the cross-talk between the lateral and normal response of the probe. Due to the low spring constant of the probe, the observed frictional contrast between the sample and the substrate can mask or amplify small height differences. Cross-talk is a common artifact experienced in contact mode and is further discussed in literature [33, 50]. To avoid the effect of cross-talk and obtain

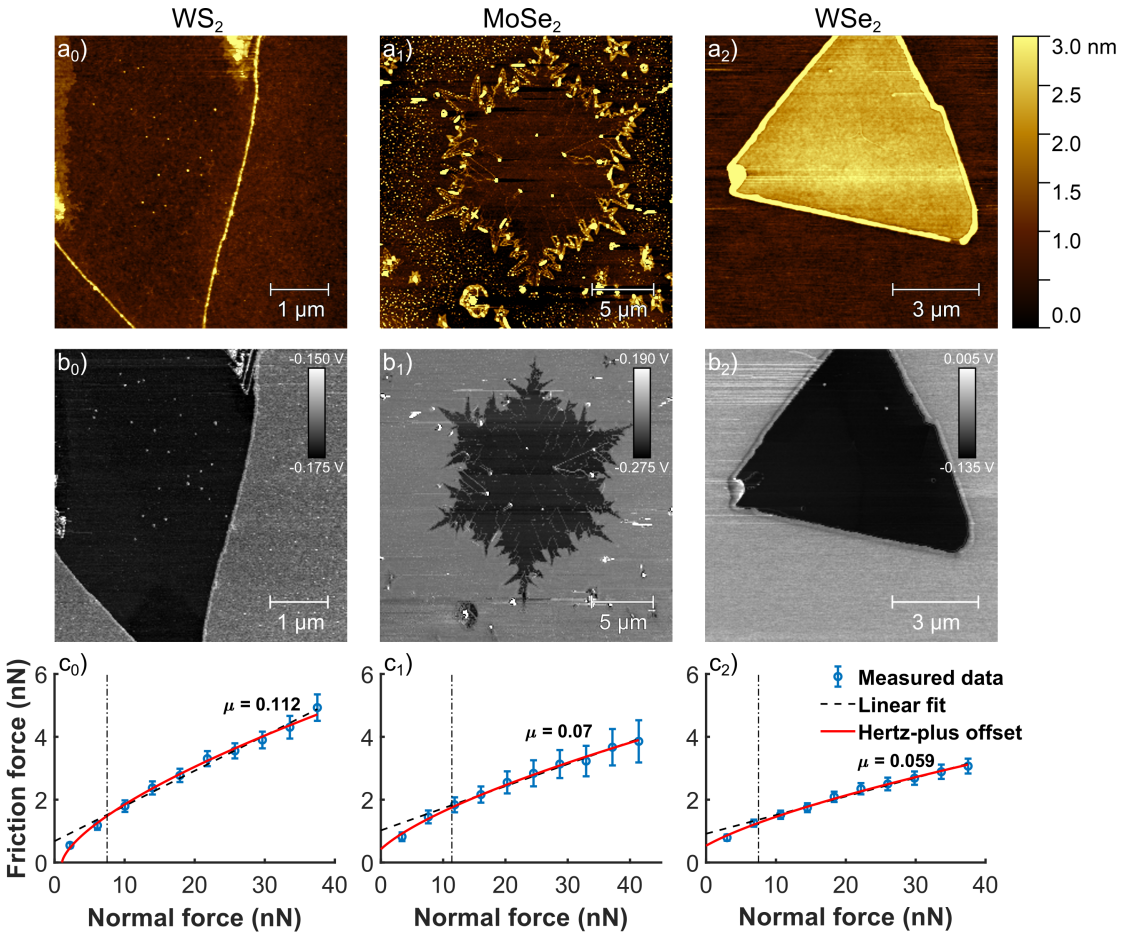

Figure 4: Surface characterisation of the analysed monolayer WS_2, $MoSe_2$ and WSe_2 flakes. Topography (a_0-a_2), corresponding friction maps (b_0-b_2) and load-dependent friction (c_0-c_2). Normal force represents the combined force of adhesion and applied load. Zero applied load is marked by a dotted dashed line.

meaningful values of the thickness, the flakes were also measured in tapping mode. The obtained thickness values of ∼0.75 nm, ∼0.78 nm and ∼0.76 nm, for WS_2, $MoSe_2$, and WSe_2, respectively, agree well with the reported values for monolayer flakes [48, 51–55].

Friction maps (Figure 4b) show high friction contrast between the flakes and the SiO_2 substrate. All the analysed TMD flakes experienced much lower friction than the substrate, indicating superior frictional characteristics. This indicates that coating a single surface in the MEMS/NEMS contacts with a TMD monolayer can offer a great performance improvement. Load dependent frictional behaviour of the three samples is shown in Figure 4c. Only the results obtained at 1 µm/s are shown here, despite performing the measurements at various sliding speeds; the speed dependence is discussed later. No stick-slip motion was observed on any of the samples. The measurements were consistent for a total of three different WS_2 and WSe_2 flakes and two separate locations on the $MoSe_2$ flake. No significant difference was observed between the loading and unloading curves on any of the samples, which can be expected for an elastic contact, where a layer has good adhesion to the substrate (Supporting Information, Figure S2). Thus, only the data with increasing normal force are shown in Figure 4c for clarity.

We observed only minor fluctuation of friction with sliding speed across the analysed range (Supporting Information, Figure S3), which can be attributed to measurement uncertainty and internal equipment error. The only obvious difference in the response is on the $MoSe_2$ sample at increasing load (Supporting Information, Figure S3b) at 0.5 Hz (0.5 µm/s). However, it is the only measurement that deviates from the rest, and it was the first measurement that was taken on that sample. Therefore, we can conclude that the difference in response was a consequence of surface or tip contamination. The amount of contamination was very low, and it was completely removed after the initial scan, which is evident from the other measurements on the same sample. Even the measurement with decreasing load (Supporting Information, Figure S3e) at 0.5 Hz, performed right after in the same area, did not show any deviation between the sliding speeds anymore. Besides that, all three samples exhibit the same behaviour, indicating that nanoscale friction of TMDs is independent of sliding speed within the analysed range.

3.3 Nanotribology: Wear resistance

The experiments above were performed at relatively low loads to prevent possible damage to the tip or to the substrate. Following that, we increased the maximum load up to 10 µN to analyse the WS_2 monolayers for potential rupture and tip wear. A pre-worn probe was used to prevent the tip shattering solely due to high pressure, which could give inconsistent results. In fact, a measurement with a new sharp probe resulted in the probe shattering at 6 µN on WS_2 (Supporting Information, Figure S4). Therefore, we only present the results obtained by the pre-worn probe here. Additionally, we performed the reference scans on the SiO_2 substrate.

We have not observed any sample wear on either SiO_2 or WS_2. However, high friction between the tip and the SiO_2 surface caused the tip to start wearing off above 1000 nN, which resulted in the transfer of material from the tip to the surface (see the insets in Figure 5a). Probe wear is quantitatively evaluated in Figure 5a; the total volume difference was determined between the surface topography after each wear measurement and the initial topography scan at 0 nN. As expected, the volume differences are negligible on WS_2, but we see an almost linear increase after 500 nN on the SiO_2.

The bars in Figure 5a show the distance to failure (e.g. the point at which we could visually notice the changes on the surface) at the loads where tip wear was observed. The total scanned distance at each load was 768 µm, indicating that even though we measured noticeable amounts of tip wear at 1000 nN, it only happened towards the end of the experiment. The distance reduced significantly at higher loads; at 1500 nN it reduced down to 40 µm whereas at 2000 nN the transfer of the material occurred after only 15 µm of sliding. Therefore, the limit of usable loads on SiO_2 is around 1000 nN. On the other hand, sliding on WS_2 did not result in similar behaviour; even near the technical limit of our setup at 10 µN, there was no tip wear (Figure 5b). The complete scans on both surfaces after all analysed loads are shown in (Supporting Information, Figure S5).

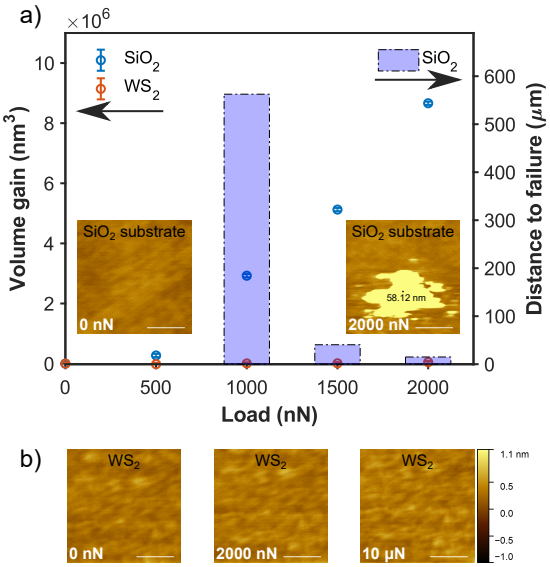

Figure 5: Tip wear on SiO_2 substrate and WS_2 samples. (a) Sample volume gain and distance to failure. The insets show the surface topography after the experiments performed on SiO_2 substrate at 0 nN and 2000 nN. (b) WS_2 monolayer surface topography after the experiments at 0 nN, 2000 nN and 10 µN. The height bar applies to all topography scans. The lateral scale bars correspond to 500 nm

.

4 Discussion

The standard approach to frictional analysis is to obtain the slope μ of the increasing friction with applied load L, similar to linear Amontons' law on the macro scale [56]. Obviously, at the nanoscale the friction does not vanish at zero load due to the effects of adhesion; therefore, the friction force at zero load F_0 needs to be considered. Adhesion is initially included in total normal force $F_N = L + F_{adh}$ [30], leading to a formulation of Amontons' law with included effects of adhesion:

$$F_f = \mu F_N + F_0. \tag{1}$$

The formulation is straight-forward and readily comparable with the approach to understanding friction on the macro-scale. However, it can only serve as an initial assessment of the analysed measurements and can only be applied in cases when the observed behaviour is linear. Its major drawbacks include general inapplicability at low loads and its dependence on the contact geometry. Furthermore, it is only applicable to compare the measurements obtained with the same probe.

By observing the friction graphs in Figure 4c, we see the linear trend from ∼10 nN onward, whereas at lower loads, the frictional response deviates from linear behaviour. Note that below 10 nN we are already entering the adhesive regime, where the surfaces are kept in contact solely by adhesion. By assuming the onset of linear behaviour at higher loads, we have only considered the data above 10 nN normal load when fitting the linear model. The resulting values of μ and F_0 are collected in Table 4.

Because adhesion plays a major role in contact properties of nanoscale contacts, a more suitable approach is to include adhesive contact models from solid mechanics [57]. Several models have been suggested to study the contact interactions in the AFM contact [30, 58, 59], proposing either JKR [60], DMT [61], or transition regime to model the adhesive contact. The benefit of these models is that they incorporate contact geometry (usually approximated by sphere-on-flat contact) and adhesion and thus allow for a much more accurate comparison between the measurements performed using different probes and systems.

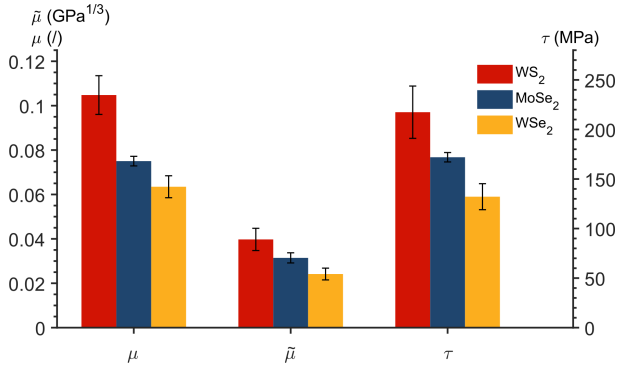

Figure 6: Averaged frictional and contact parameters.

Table 4: Contact properties of TMD samples measured by LFM.

Sample	μ (/)	F_0 (nN)	$\tilde{\mu}$ (GPa$^{1/3}$)	τ (MPa)	F_{off} (nN)	F_{adh}(nN)	R^2 (/)
WS_2	0.112	0.7	0.0413 ± 0.0014	226.1	1.1	7.5	0.9947
$MoSe_2$	0.073	0.8	0.0308 ± 0.0015	168.6	0.3	11.4	0.9910
WSe_2	0.059	0.9	0.0255 ± 0.0009	139.6	-2.9	7.5	0.9955

One of such models, which is commonly [27, 28] used to fit lateral force data is Hertz-plus-offset model for a sphere on flat contact [30]:

$$F_f = \tilde{\mu} R^{2/3} (F_N - F_{off})^{2/3}. \tag{2}$$

The model introduces the effective coefficient of friction for point-like contact $\tilde{\mu} = \pi\tau/K^{2/3}$, where τ is contact shear strength and K is the effective contact elastic modulus. $\tilde{\mu}$ is a more valid coefficient for comparison of the frictional behaviour of materials on a small scale than the conventional coefficient of friction because it is independent of the contact geometry. The force of adhesion is initially approximated by measuring pull-off force ($F_{adh} \approx F_{pull-off}$, which leads to $F_N = L + F_{pull-off}$). However, due to the uncertainty in the determination of pull-off force, an offset ($F_{off} \ll F_{pull-off}$) is introduced, which corrects for any discrepancy in adhesion measurement. R is the radius of the probe, which was determined by scanning a standard calibration grating TGT1 (ND-MDT, Russia), and calculated using the envelope method [62]. The obtained radius was 33.4 nm. As the manufacturer specified radius for a new probe is less than 10 nm, this indicates some wear occurred throughout the measurements. However, because no visible signs of wear were observed on the scans during friction measurements, we can assume that the majority of the probe wear occurred during the initial contact of the tip with the sample and throughout the initial topography measurements. As reported by J. Liu et al. [63] and D.S. Grierson et al. [64], the sharp apex of Si tip could shatter almost immediately after contact with the surface. A slight increase of the probe radius after the measurements is therefore expected.

The results of the fit are summarised in Table 4. Hertz-plus-offset is equivalent to DMT contact model, which is consistent with many AFM measurements, when the surfaces are atomically flat, sufficiently hard, and can be approximated by a sphere on flat contact [30]. We observe a very good fit to the model ($R^2 > 0.99$, $F_{off} < F_{adh}$) for all three samples, which further confirms wear-less friction and fully elastic contact and thus shows that the friction is proportional to the contact area.

The averaged frictional parameters of the measurements on all three WS_2 and WSe_2 flakes and on both regions on the $MoSe_2$ flake, are shown in Figure 6. All three samples exhibit low friction, but there are observable differences between the samples. Both selenium containing samples showed lower friction than

the sulphur-based monolayer (WS_2). This indicates that the chalcogenide atom has a major influence on the friction of TMD monolayers, although the influence of the metal atom is not negligible. Thus, we can conclude that friction of clean layers is mainly driven by the interatomic forces between the contacting bodies, with structural properties of the layers taking a secondary role.

Since there were no large differences in measured pull-off forces among the three TMD samples, we can conclude that the difference in friction between different samples was not related to difference in adhesion. In fact, the same pull-off force was measured on samples with the highest and the lowest measured friction.

Comparing our measured values with the values of $\tilde{\mu}$ from the literature, we see that the values obtained on TMDs are substantially lower than the majority reported in Table 1, except for highly oriented pyrolytic graphite (HOPG) measured in argon atmosphere. Due to the high quality of HOPG crystals, they contain fewer surface defects compared to CVD grown monolayers, which are more prone to defects due to shorter time scales used for deposition [65]. Furthermore, our measurements were performed in air; therefore, we can expect some degree of organics and water adsorbed on the surface [66]. Both effects can contribute significantly to the final frictional response. Therefore, eliminating them on TMD surfaces could further decrease friction and make them potentially more comparable with HOPG. Nevertheless, the quantitative friction observed on all the TMD samples was very low.

5 Conclusions

We have shown that all the measured TMD monolayer samples exhibited low nanoscale friction, therefore indicating good tribological behaviour. The exact elemental structure of the clean samples had some effect on the frictional response; however, all three monolayers showed similar behaviour. WS_2 monolayer experienced the highest values of the lateral force and WSe_2 experienced the lowest. The results indicate that selenides would result in lower friction than sulphides. The samples also did not show any dependence on sliding speed. Furthermore, we have shown that the TMD monolayers can significantly reduce and delay the onset of wear in high load applications.

We can conclude that precisely selecting a single TMD for a specific sliding application is less important than ensuring that the deposited monolayer crystal would be of high quality, contain a low number of defects and be free of contamination.

Acknowledgements

This work is supported by Horizon 2020 MSCA ITN project Solution No. 721642.

T.P. also acknowledges support from the project OPVVV Novel nanostructures for engineering applications No. CZ.02.1.01/0.0/0.0/16_026/0008396.

References

[1] Novoselov, K.S., Geim, A.K., Morozov, S.V., Jiang, D., Zhang, Y., Dubonos, S.V., et al. Electric Field Effect in Atomically Thin Carbon Films. Science 2004;306(5696):666–669. doi:10.1126/science.1102896.

[2] Reina, A., Jia, X., Ho, J., Nezich, D., Son, H., Bulovic, V., et al. Large area, few-layer graphene films on arbitrary substrates by chemical vapor deposition. Nano Letters 2009;9(1):30–35. doi:10.1021/nl801827v.

[3] Yu, Q., Lian, J., Siriponglert, S., Li, H., Chen, Y.P., Pei, S.S.. Graphene segregated on Ni surfaces and transferred to insulators. Applied Physics Letters 2008;93(11):1–4. doi:10.1063/1.2982585.

[4] Geim, A.K., Novoselov, K.S.. The rise of graphene. Nature Materials 2007;6(3):183–191. doi:10.1038/nmat1849.

[5] Choi, W., Choudhary, N., Han, G.H., Park, J., Akinwande, D., Lee, Y.H.. Recent development of two-dimensional transition metal dichalcogenides and their applications. Materials Today 2017;20(3):116–130. doi:10.1016/j.mattod.2016.10.002.

[6] Gupta, A., Sakthivel, T., Seal, S.. Recent development in 2D materials beyond graphene. Progress in Materials Science 2015;73:44–126. doi:10.1016/j.pmatsci.2015.02.002.

[7] Li, H.H., Yin, Z., He, Q., Li, H.H., Huang, X., Lu, G., et al. Fabrication of single- and multilayer MoS 2 film-based field-effect transistors for sensing NO at room temperature. Small 2012;8(1):63–67. doi:10.1002/smll.201101016.

[8] Spear, J.C., Ewers, B.W., Batteas, J.D.. 2D-nanomaterials for controlling friction and wear at interfaces. Nano Today 2015;10(3):301–314. doi:10.1016/j.nantod.2015.04.003.

[9] de Boer, M., Mayer, T.. Tribology of MEMS. MRS Bulletin 2001;26(4):302–304. doi:10.1557/mrs2001.65.

[10] Maboudian, R., Howe, R.T.. Critical review: Adhesion in surface micromechanical structures. Journal of Vacuum Science and Technology B: Microelectronics and Nanometer Structures 1997;15(1):1–20. doi:10.1116/1.589247.

[11] Maboudian, R., Ashurst, W.R., Carraro, C.. Tribological challenges in micromechanical systems. Tribology Letters 2002;12(2):95–100. doi:10.1023/A:1014044207344.

[12] Bhushan, B.. Nanotribology and nanomechanics of MEMS/NEMS and BioMEMS/BioNEMS materials and devices. Microelectronic Engineering 2007;84(3):387–412. doi:10.1016/j.mee.2006.10.059.

[13] Guo, W., Yin, J., Qiu, H., Guo, Y., Wu, H., Xue, M.. Friction of low-dimensional nanomaterial systems. Friction 2014;2(3):209–225. doi:10.1007/s40544-014-0064-0.

[14] Winer, W.O.. Molybdenum Disulpide As a Lurricant: a Review of Fundamental Knowledge. Wear 1967;10:422–452.

[15] Spalvins, T., Przybyszewski, J.S.. Deposition of sputtered molybdenum disulphide films and friction characteristics of such films in vacuum. Vacuum 1968;18(8):496. doi:10.1016/0042-207X(68)90504-6.

[16] Przybyszewski, J.S., Spalvins, T.. Friction and contact resistance during sliding in vacuum of some low-resistivity metals lubricated with sputtered molybdenum disulfide films. Nasa Technical Note 1969;.

[17] Jamison, W.E., Cosgrove, S.L.. Friction Characteristics of Transition-Metal Disulfides and Diselenides. A S L E Transactions 1971;14(1):62–72. doi:10.1080/05698197108983228.

[18] Bergmann, E., Melet, G., Müller, C., Simon-Vermot, A.. Friction properties of sputtered dichalcogenide layers. Tribology International 1981;14(6):329–332. doi:10.1016/0301-679X(81)90100-6.

[19] Lee, C., Li, Q., Kalb, W., Liu, X.Z., Berger, H., Carpick, R.W., et al. Frictional Characteristics of Atomically Thin Sheets. Science 2010;328(5974):76–80. doi:10.1126/science.1184167.

[20] Polcar, T., Cavaleiro, A.. Review on self-lubricant transition metal dichalcogenide nanocomposite coatings alloyed with carbon. Surface and Coatings Technology 2011;206(4):686–695. doi:10.1016/j.surfcoat.2011.03.004.

[21] A.R. Lansdown, . Molybdenum Disulphide Lubrication. 1st ed.; Elsevier; 1999.

[22] Berman, D., Erdemir, A., Sumant, V.A.. Approaches for Achieving Superlubricity in Two-Dimensional Materials. ACS Nano 2018;12(3):2122–2137. doi:10.1021/acsnano.7b09046.

[23] Szlufarska, I., Chandross, M., Carpick, R.W.. Recent advances in single-asperity nanotribology. Journal of Physics D: Applied Physics 2008;41(12):123001. doi:10.1088/0022-3727/41/12/123001.

[24] Dienwiebel, M., Verhoeven, G.S., Pradeep, N., Frenken, J.W., Heimberg, J.A., Zandbergen, H.W.. Superlubricity of graphite. Physical Review Letters 2004;92(12):1–4. doi:10.1103/PhysRevLett.92.126101.

[25] Lin, L.Y., Kim, D.E., Kim, W.K., Jun, S.C.. Friction and wear characteristics of multi-layer graphene films investigated by atomic force microscopy. Surface and Coatings Technology 2011;205(20):4864–4869. doi:10.1016/j.surfcoat.2011.04.092.

[26] Fang, L., Liu, D.M., Guo, Y., Liao, Z.M.Z.M., Luo, J.B.J.B., Wen, S.Z.S.Z.. Thickness dependent friction on few-layer MoS2, WS2, and WSe2. Nanotechnology 2017;28(24):245703. doi:10.1088/1361-6528/aa712b.

[27] Zekonyte, J., Cavaleiro, A., Polcar, T.. Frictional properties of self-adaptive chromium doped tungsten-sulfur- carbon coatings at nanoscale. Applied Surface Science 2014;303:381–387. doi:10.1016/j.apsusc.2014.03.010.

[28] Zekonyte, J., Polcar, T.. Friction Force Microscopy Analysis of Self-Adaptive W-S-C Coatings: Nanoscale Friction and Wear. ACS Applied Materials and Interfaces 2015;7(38):21056–21064. doi:10.1021/acsami.5b05546.

[29] Elinski, M.B., Liu, Z., Spear, J.C., Batteas, J.D.. 2D or not 2D? the impact of nanoscale roughness and substrate interactions on the tribological properties of graphene and MoS2. Journal of Physics D: Applied Physics 2017;50(10). doi:10.1088/1361-6463/aa58d6.

[30] Schwarz, U.D., Zwörner, O., Köster, P., Wiesendanger, R.. Quantitative analysis of the frictional properties of solid materials at low loads. I. Carbon compounds. Physical Review B 1997;56(11):6987–6996. doi:10.1103/PhysRevB.56.6987.

[31] Schwarz, U.D., Zwörner, O., Köster, P., Wiesendanger, R.. Quantitative analysis of the frictional properties of solid materials at low loads. II. Mica and germanium sulfide. Physical Review B - Condensed Matter and Materials Physics 1997;56(11):6997–7000. doi:10.1103/PhysRevB.56.6997.

[32] Hutter, J.L., Bechhoefer, J.. Calibration of atomic-force microscope tips. Review of Scientific Instruments 1993;64(7):1868–1873. doi:10.1063/1.1143970.

[33] Ogletree, D.F., Carpick, R.W., Salmeron, M.. Calibration of frictional forces in atomic force microscopy. Review of Scientific Instruments 1996;67(9):3298–3306. doi:10.1063/1.1147411.

[34] Berkdemir, A., Gutiérrez, H.R., Botello-Méndez, A.R., Perea-López, N., Elías, A.L., Chia, C.I., et al. Identification of individual and few layers of WS2 using Raman Spectroscopy. Scientific Reports 2013;3:1–8. doi:10.1038/srep01755.

[35] Lv, Y., Huang, F., Zhang, L., Weng, J., Zhao, S., Ji, Z.. Preparation and Photoluminescence of Tungsten Disulfide Monolayer. Coatings 2018;8(6):205. doi:10.3390/coatings8060205.

[36] Martinez, H., Benayad, A., Gonbeau, D., Vinatier, P., Pecquenard, B., Levasseur, A.. Influence of the cation nature of high sulfur content oxysulfide thin films MO S (M=W, Ti) studied by XPS. Applied Surface Science 2004;236(1-4):377–386. doi:10.1016/j.apsusc.2004.05.010.

[37] Cattelan, M., Markman, B., Lucchini, G., Das, P.K., Vobornik, I., Robinson, J.A., et al. New Strategy for the Growth of Complex Heterostructures Based on Different 2D Materials. Chemistry of Materials 2015;27(11):4105–4113. doi:10.1021/acs.chemmater.5b01170.

[38] Reale, F., Palczynski, P., Amit, I., Jones, G.F., Mehew, J.D., Bacon, A., et al. High-Mobility and High-Optical Quality Atomically Thin WS 2. Scientific Reports 2017;7(1):14911. doi:10.1038/s41598-017-14928-2.

[39] Shaw, J.C., Zhou, H., Chen, Y., Weiss, N.O., Liu, Y., Huang, Y., et al. Chemical vapor deposition growth of monolayer MoSe 2 nanosheets. Nano Research 2014;7(4):511–517. doi:10.1007/s12274-014-0417-z.

[40] Xia, J., Huang, X., Liu, L.Z., Wang, M., Wang, L., Huang, B., et al. CVD synthesis of large-area, highly crystalline MoSe2 atomic layers on diverse substrates and application to photodetectors. Nanoscale 2014;6(15):8949–8955. doi:10.1039/c4nr02311k.

[41] O'Brien, M., McEvoy, N., Hanlon, D., Lee, K., Gatensby, R., Coleman, J.N., et al. Low wavenumber Raman spectroscopy of highly crystalline MoSe 2 grown by chemical vapor deposition. physica status solidi (b) 2015;252(11):2385–2389. doi:10.1002/pssb.201552225.

[42] Huang, J., Liu, H., Jin, B., Liu, M., Zhang, Q., Luo, L., et al. Large-area snow-like MoSe 2 monolayers: synthesis, growth mechanism, and efficient electrocatalyst application. Nanotechnology 2017;28(27):275704. doi:10.1088/1361-6528/aa7533.

[43] Zhao, Y., Lee, H., Choi, W., Fei, W., Lee, C.J.. Large-area synthesis of monolayer MoSe 2 films on SiO 2 /Si substrates by atmospheric pressure chemical vapor deposition. RSC Advances 2017;7(45):27969–27973. doi:10.1039/C7RA03642F.

[44] Wang, B.B., Ostrikov, K., Van Der Laan, T., Zheng, K., Shao, R., Zhu, M.K., et al. Growth and photoluminescence of oriented MoSe2 nanosheets produced by hot filament CVD. RSC Advances 2016;6(43):37236–37245. doi:10.1039/c6ra05737c.

[45] Roy, A., Movva, H.C.P., Satpati, B., Kim, K., Dey, R., Rai, A., et al. Structural and Electrical Properties of MoTe2 and MoSe2 Grown by Molecular Beam Epitaxy. ACS Applied Materials & Interfaces 2016;8:7396–7402. doi:10.1021/acsami.6b00961.

[46] Wang, X., Gong, Y., Shi, G., Chow, W.L., Keyshar, K., Ye, G., et al. Chemical vapor deposition growth of crystalline monolayer MoSe2. ACS Nano 2014;8(5):5125–5131. doi:10.1021/nn501175k.

[47] Li, H., Lu, G., Wang, Y., Yin, Z., Cong, C., He, Q., et al. Mechanical exfoliation and characterization of single- and few-layer nanosheets of WSe2, TaS2, and TaSe2. Small 2013;9(11):1974–1981. doi:10.1002/smll.201202919.

[48] Huang, J.K., Pu, J., Hsu, C.L., Chiu, M.H., Juang, Z.Y., Chang, Y.H., et al. Large-area synthesis of highly crystalline WSe2 monolayers and device applications. ACS Nano 2014;8(1):923–930. doi:10.1021/nn405719x.

[49] Huang, J., Yang, L., Liu, D., Chen, J., Fu, Q., Xiong, Y., et al. Large-area synthesis of monolayer WSe2 on a SiO2/Si substrate and its device applications. Nanoscale 2015;7(9):4193–4198. doi:10.1039/c4nr07045c.

[50] Gołek, F., Mazur, P., Ryszka, Z., Zuber, S.. AFM image artifacts. Applied Surface Science 2014;304:11–19. doi:10.1016/j.apsusc.2014.01.149.

[51] Liu, P., Luo, T., Xing, J., Xu, H., Hao, H., Liu, H., et al. Large-Area WS2 Film with Big Single Domains Grown by Chemical Vapor Deposition. Nanoscale Research Letters 2017;12(1):558. doi:10.1186/s11671-017-2329-9.

[52] Fu, Q., Wang, W., Yang, L., Huang, J., Zhang, J., Xiang, B.. Controllable synthesis of high quality monolayer WS2 on a SiO2/Si substrate by chemical vapor deposition. RSC Adv 2015;5(21):15795–15799. doi:10.1039/C5RA00210A.

[53] Ghosh, R., Kim, J.S., Roy, A., Chou, H., Vu, M., Banerjee, S.K., et al. Large area chemical vapor deposition growth of monolayer MoSe2 and its controlled sulfurization to MoS2. Journal of Materials Research 2016;:1–6doi:10.1557/jmr.2016.7.

[54] Chang, Y.h., Zhang, O.W., Zhu, O.Y., Han, Y., Pu, J., Chang, J.k., et al. Monolayer MoSe2 Grown by Chemical Vapor Deposition for Fast Photodetection. ACS Nano 2014;8(8):8582–8590. doi:10.1021/nn503287m.

[55] Liu, W., Kang, J., Sarkar, D., Khatami, Y., Jena, D., Banerjee, K.. Role of metal contacts in designing high-performance monolayer n-type WSe2 field effect transistors. Nano Letters 2013;13(5):1983–1990. doi:10.1021/nl304777e.

[56] Bowden, F.P., Tabor, D.. The Friction and Lubrication of Solids. 1st ed.; Oxford: Clarendon Press; 1950.

[57] Kopycinska-Müller, M., Geiss, R.H., Hurley, D.C.. Contact mechanics and tip shape in AFM-based nanomechanical measurements. Ultramicroscopy 2006;106(6):466–474. doi:10.1016/j.ultramic.2005.12.006.

[58] Carpick, R.W., Ogletree, D., Salmeron, M.. A General Equation for Fitting Contact Area and Friction vs Load Measurements. Journal of Colloid and Interface Science 1999;211(2):395–400. doi:10.1006/jcis.1998.6027.

[59] Schwarz, U.D.. A generalized analytical model for the elastic deformation of an adhesive contact between a sphere and a flat surface. Journal of Colloid and Interface Science 2003;261(1):99–106. doi:10.1016/S0021-9797(03)00049-3.

[60] Johnson, K.L., Kendall, K., Roberts, A.D.. Surface Energy and the Contact of Elastic Solids. Proceedings of the Royal Society A: Mathematical, Physical and Engineering Sciences 1971;324(1558):301–313. doi:10.1098/rspa.1971.0141.

[61] Derjaguin, V.B., Muller, V.M., Toporov, Y.P.. Effect of contact deformations on the adhesion of particles. Journal of Colloid And Interface Science 1975;53(2):314–326. doi:10.1016/0021-9797(75)90018-1.

[62] Keller, D.J., Franke, F.S.. Envelope reconstruction of probe microscope images. Surface Science 1993;294(3):409–419. doi:10.1016/0039-6028(93)90126-5.

[63] Liu, J., Notbohm, J.K., Carpick, R.W., Turner, K.T.. Method for characterizing nanoscale wear of atomic force microscope tips. ACS Nano 2010;4(7):3763–3772. doi:10.1021/nn100246g.

[64] Grierson, D.S., Liu, J., Carpick, R.W., Turner, K.T.. Adhesion of nanoscale asperities with power-law profiles. Journal of the Mechanics and Physics of Solids 2013;61(2):597–610. doi:10.1016/j.jmps.2012.09.003.

[65] Lin, Z., Carvalho, B.R., Kahn, E., Lv, R., Rao, R., Terrones, H., et al. Defect engineering of two-dimensional transition metal dichalcogenides. 2D Materials 2016;3(2). doi:10.1088/2053-1583/3/2/022002.

[66] Gao, J., Li, B., Tan, J., Chow, P., Lu, T.M., Koratkar, N.. Aging of Transition Metal Dichalcogenide Monolayers. ACS Nano 2016;10(2):2628–2635. doi:10.1021/acsnano.5b07677.